2007

Downscaling Daily Maximum and Minimum Air Temperature in the Midwestern USA: A Hybrid Empirical Approach

Justin T. Schoof
Southern Illinois University Carbondale, jschoof@siu.edu

S C. Pryor
Indiana University Bloomington

S M. Robeson
Indiana University Bloomington

INTERNATIONAL JOURNAL OF CLIMATOLOGY
Int. J. Climatol. **27**: 439–454 (2007)
Published online 28 September 2006 in Wiley InterScience
(www.interscience.wiley.com) DOI: 10.1002/joc.1412

RMetS
ROYAL METEOROLOGICAL SOCIETY

Downscaling daily maximum and minimum temperatures in the midwestern USA: a hybrid empirical approach

J. T. Schoof,[a]* S. C. Pryor[b] and S. M. Robeson[b]
[a] *Department of Geography and Environmental Resources, Southern Illinois University, Carbondale, IL, 62901*
[b] *Atmospheric Science Program, Department of Geography, Indiana University, Bloomington, IN, 47405*

Abstract:

A new hybrid empirical downscaling technique is presented and applied to assess 21st century projections of maximum and minimum daily surface air temperatures (T_{max}, T_{min}) over the Midwestern USA. Our approach uses multiple linear regression to downscale the seasonal variations of the mean and standard deviation of daily T_{max} and T_{min} and the lag-0 and lag-1 correlations between daily T_{max} and T_{min} based on GCM simulation of the large-scale climate. These downscaled parameters are then used as inputs to a stochastic weather generator to produce time series of the daily T_{max} and T_{min} at 26 surface stations, in three time periods (1990–2001, 2020–2029, and 2050–2059) based on output from two coupled GCMs (HadCM3 and CGCM2). The new technique is demonstrated to exhibit better agreement with surface observations than a transfer-function approach, particularly with respect to temperature variability. Relative to 1990–2001 values, downscaled temperature projections for 2020–2029 indicate increases that range (across stations) from 0.0 K to 1.7 K (T_{max}) and 0.0 K to 1.5 K (T_{min}), while increases for 2050–2059 relative to 1990–2001 range from 1.4 K to 2.4 K (T_{max}) and 0.8 to 2.2K (T_{min}). Although the differences between GCMs demonstrate the continuing uncertainty of GCM-based regional climate downscaling, the inclusion of weather-generator parameters represents an advancement in downscaling methodology. Copyright © 2006 Royal Meteorological Society

KEY WORDS empirical downscaling; stochastic weather generator; regional climate change

Received 7 May 2006; Revised 13 July 2006; Accepted 13 July 2006

INTRODUCTION

Coupled atmosphere-ocean general circulation models (GCMs) indicate that increases in atmospheric greenhouse gas concentrations will result in global average surface air temperature increases of a few degrees Celsius by the end of the 21st century (Cubasch *et al*., 2001). GCMs most accurately simulate climate at the annual and seasonal time scales over broad continental scales (McAveney *et al*., 2001), hence, downscaling techniques have been developed to relate information at large scales (at which GCMs are more reliable) to local-scale climate information, allowing generation of regional climate change scenarios (Wilby and Wigley (1997) and Giorgi *et al*., 2001).

The most common empirical downscaling approaches are based on transfer functions, which use direct relationships between free-atmosphere predictors and surface variables of interest. These transfer functions vary in complexity from simple interpolation and regression models (Kim *et al*., 1984; Sailor and Li, 1999) to artificial neural networks (Mpelasoka *et al*., 2001; Schoof and Pryor, 2001), and typically focus on changes in the central tendency of surface variables. Weather typing approaches, which relate surface climate variables to the large-scale state (usually defined in terms of circulation), have also been used effectively (Goodess and Palutikof, 1998; Schnur and Lettenmaier, 1998; Bellone *et al*., 2000; Bardossy *et al*., 2002) and are based on the assumption that the surface climate response varies according to large-scale weather type. Another alternative is the use of weather generators, a special class of random number generators that produce realistic surface climate sequences (e.g. Wilks, 1992; Wilks, 1999). When run with perturbed parameters, these models are capable of producing arbitrarily long sequences of surface climate variables consistent with the climate change signal produced by a GCM, which can be used to examine changes in both the mean climate and climate variability (Wilks and Wilby, 1999).

Most weather-generator downscaling applications have relied on adjusting the weather-generator parameters in a way consistent with the changes in GCM-simulated monthly means and variances. In this study, we develop, apply, and evaluate a new hybrid downscaling method for temperature on the basis of regression analysis of weather-generator parameters from daily GCM output. The hybrid approach focuses not only on changes in temperature means and variances, but also

* Correspondence to: J. T. Schoof, Department of Geography and Environmental Resources, Southern Illinois University, Carbondale, IL, 62901; e-mail: jschoof@siu.edu

on changes in auto- and cross-correlation matrices used in stochastic weather generators. Scenarios that include the combined effects of changes in mean, variance, and autocorrelation are crucial for impact studies focused on agriculture or human health (e.g. heat wave frequency).

STUDY REGION

The geographic focus of this study is the Midwest region of the USA, which extends from approximately 35° to 50 °N latitude and from 75° to 95 °W longitude (Figure 1), although the techniques developed have broader applications. According to Folland *et al*. (2001), the northern part of the study region (i.e. the upper Great Lakes) has warmed by approximately 2 K over the past 100 years, while the southern and eastern parts of the region have warmed only slightly or have even cooled. However, during the last quarter century, all parts of the region have warmed (trends of 0.4–0.8 K per decade), with the largest warming during winter.

The study region is highly sensitive to climate change for several reasons. It is a major agricultural center, producing a large proportion of the nation's corn and soybeans. Also, with the exception of the polar ice caps, the Great Lakes are the world's largest source of fresh water and, in addition to providing drinking water and hydroelectric power to the region, serve as a major transportation system. Key climate change issues for the Midwest region of the United States include reductions in lake and river levels, increases in heat related stress and mortality, and shifts in agricultural productivity (Sousounis and Albercook, 2000). Heat related mortality in this region has received a great deal of attention due to major regional heat waves during both 1980 and 1995 (Changnon *et al*., 1996; Karl and Knight, 1997; Smoyer, 1998) and continued heat wave vulnerability despite increases in public awareness and the use of air conditioning (Smoyer, 1998). Accordingly, we focus here on daily maximum and minimum surface air temperature (T_{max} and T_{min}), although future work will consider additional variables.

DATA

Reanalysis data

In this research, data from both the NCEP/NCAR (Kalnay *et al*., 1996) and ECMWF (Gibson *et al*., 1997; Uppala *et al*., 2005) reanalysis products are used to train the downscaling models and evaluate GCM simulations of the downscaling predictors. These data are gridded at a horizontal resolution of 2.5° × 2.5°, with either daily or sub-daily availability at multiple atmospheric levels for at least 1958–2001. Daily upper-level specific humidity data were not available from the NCEP/NCAR reanalysis at the time of the analysis presented here, and we therefore use ECMWF specific humidity data. For other large-scale variables, data are extracted from the NCEP/NCAR reanalysis.

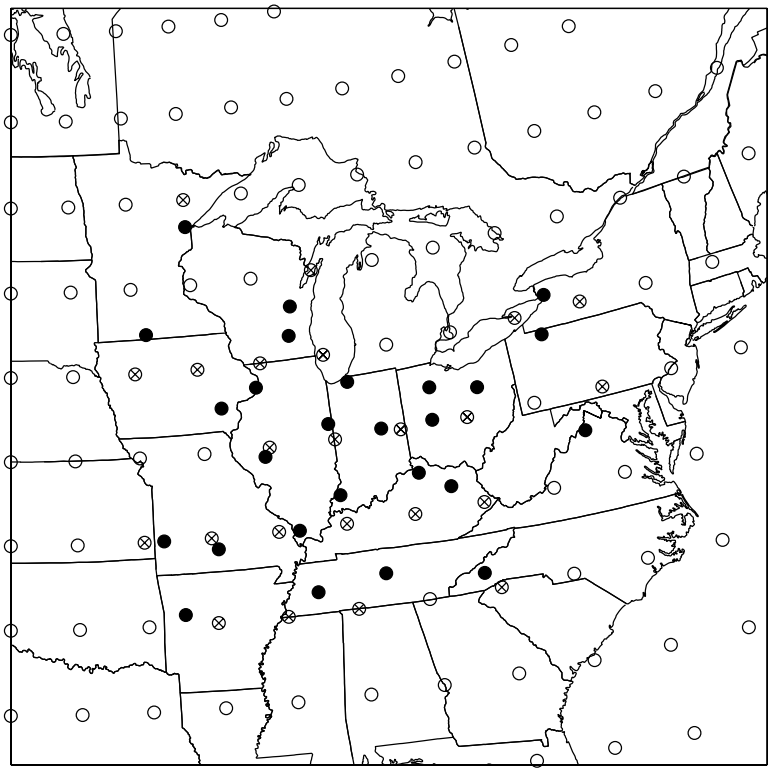

Figure 1. Map of the Midwest region of the United States showing the locations of the predictor grid cells (NCEP/NCAR and ECMWF reanalysis, HadCM3, and CGCM2) (○), and USHCN/D surface stations (●). Reanalysis/GCM grid cells used for downscaling (those nearest to the surface stations) are depicted by '×'. See Section 3 for a complete description of each data set

DOI: 10.1002/joc

Surface station data

Historical surface temperature data are susceptible to a number of biases and inhomogeneities resulting from changes in the station environment or observing practices (e.g. urbanization, station moves, instrumentation and time of observation changes; Jones, 1994; Jones *et al*., 1997; Peterson *et al*., 1998). Hence, we use data from the Daily United States Historical Climatology Network (USHCN/D; Easterling *et al*., 1999), and include only stations with a data record that is at least 95% complete over the period 1958–2001 and at least 90% complete within each year. To ensure consistency between the station data and large-scale free-atmosphere predictors, only stations with a consistent observation time are included in this study, although the observation times are allowed to vary between stations. With these constraints, we have selected 26 stations within the study region (Figure 1, Table I) for which daily maximum and minimum air temperatures are available for the period 1958–2001.

General circulation model (GCM) data

Because substantial differences exist between projections from climate models, use of a single model does not provide results that adequately reflect the uncertainty inherent in regional climate scenario generation (Cubasch *et al*., 2001). Therefore, in this study, output from transient simulations from two GCMs is used: (1) the Hadley Centre 3rd generation coupled oceanic-atmospheric general circulation model (HadCM3; Gordon *et al*., 2000; Pope *et al*., 2000) and (2) the Canadian Centre for Climate Modelling and Analysis (CCCma) 2nd Generation coupled general circulation model (CGCM2; Flato *et al*., 2000; Flato and Boer, 2001). HadCM3 and CGCM2 are chosen to provide a range of characteristics associated with coupled GCMs and are also the models used for the US National Assessment of the Potential Consequences of Climate Variability and Change (National Assessment Synthesis Team, 2000). HadCM3 is a Cartesian model (approximate horizontal resolution of 2.5° latitude ×3.75° longitude, with 19 vertical levels), whereas CGCM2 is a spectral model (T32, approximate horizontal resolution of 3.75° latitude ×3.75° longitude, with 10 vertical levels). Also, CGCM2 employs flux adjustments (Hansen *et al*., 1984), while HadCM3 has slightly higher oceanic resolution (1.25° × 1.25° *vs*. 1.8° × 1.8°) and does not employ flux adjustments.

Prior to use in this study, both GCM grids were linearly interpolated to the 2.5° × 2.5° reanalysis grid (Figure 1) using an inverse–distance based interpolation algorithm. The use of this interpolation procedure is based on the assumption that changes in the GCM-simulated variables between grid points occur at a constant rate over space. While this may introduce small errors into the GCM fields, they are likely to be negligible given the relatively smooth topography of the study region. Also, output from HadCM3, archived with a 360-day year, was linearly projected onto a 365-day year for comparison with observed data and output from CGCM2.

The GCM experiments used here were conducted using the SRES A2 emissions scenario (IPCC, 2000), which results in global carbon dioxide (CO_2) emissions from industry and energy in 2100 that are almost 4 times the 1900 value and emissions from land use change by 2100 that are close to zero, leading to a global CO_2 emission in 2100 of almost 28 GtC yr^{-1}. This emissions scenario equates to a moderate to high greenhouse gas cumulative emission for 1990–2100 as a result of projected population growth and fairly slow introduction of alternative technologies, and is used in this study to provide an upper bound on likely climate change and hence a high signal to noise ratio when comparing current and future climates. We focus on two periods from the transient GCM experiments: 2020–2029 and 2050–2059. These periods correspond to approximate doubling and tripling of emissions, respectively, owing to industrial consumption of fossil fuels, and increases in atmospheric CO_2-equivalent concentrations of approximately 20–25% and 60–65% relative to the 1990 values.

Table I. List of the 26 USHCN/D stations used in this study

Station Name	Lat (°N)	Lon (°W)	Station Name	Lat (°N)	Lon (°W)
Subiaco, AR	35.30	93.66	Lamar, MO	37.51	94.27
Anna, IL	37.47	89.24	Mountain Grove, MO	37.16	92.27
Hoopston, IL	40.47	87.67	Buffalo, NY	42.92	78.74
Jacksonville, IL	39.74	90.20	Waynesville, NC	35.49	82.97
Anderson, IN	40.11	85.72	Findlay, OH	41.05	83.67
LaPorte, IN	41.61	86.72	Urbana, OH	40.11	83.79
Princeton, IN	38.36	87.59	Wooster, OH	40.79	81.92
Clinton, IA	41.80	90.27	Warren, PA	41.86	79.16
Washington, IA	41.29	91.69	Jackson, TN	35.62	88.84
Farmers, KY	38.12	83.55	Murfreesboro, TN	35.92	86.37
Williamstown, KY	38.66	84.62	Woodstock, VA	38.91	78.47
Cloquet, MN	46.71	92.52	Oshkosh, WI	44.04	88.55
Fairmont, MN	43.64	94.47	Watertown, WI	43.19	88.74

DOI: 10.1002/joc

METHODOLOGY

The downscaling methodology presented here is based on a modified version of a common stochastic weather generator, WGEN (Richardson and Wright, 1984). The WGEN model traditionally generates daily values of precipitation occurrence (binary), precipitation amount, T_{max}, T_{min}, and solar radiation using parameters estimated from observed data. Since the variables of interest in this study are T_{max} and T_{min}, precipitation and solar radiation were not simulated, resulting in a modified version of WGEN. To simulate T_{max} and T_{min}, WGEN requires only the daily means and standard deviations of the two variables and the lag-0 and lag-1 cross correlations between T_{max} and T_{min}. The latter may be either defined separately for each month or specified on a daily basis by fitting smoothed curves to the monthly values. In the following subsections, we demonstrate that these parameters can be derived from current or transient GCM simulations using multiple linear regression methods. The downscaled parameters are then used to produce surface T_{max} and T_{min} sequences consistent with the model projections using the WGEN model. Note that, on the basis of findings presented in a previous study (Schoof and Robeson, 2003), all weather-generator parameters were computed separately for each station and allowed to vary throughout the year.

Downscaling of the seasonal cycles of T_{max} and T_{min}

As described above, WGEN requires the daily means and standard deviations of the two variables and the lag-0 and lag-1 cross correlations between T_{max} and T_{min}, hence our approach to downscaling the daily means and standard deviations of T_{max} and T_{min} begins with downscaling of the means and standard deviations of the daily values at the monthly timescale using the 1958–2001 means and standard deviations of large-scale climate parameters ($n = 12 \times 44 = 528$). Potential predictors were drawn from a literature review of previous research, noting the constraint that they are available from the GCMs with daily temporal resolution (Table II). The predictors are chosen to reflect (1) atmospheric circulation, (2) lower atmospheric air temperature, and (3) atmospheric humidity. The geostrophic components of flow and vorticity are derived from the sea level pressure field using previously published methods and are used as proxies for near-surface winds associated with thermal advection (see Dessouky and Jenkinson, 1975; Jenkinson and Collison, 1977; Jones *et al*., 1993).

A key prerequisite for use of grid cell GCM data in empirical downscaling is that the GCM accurately reproduces the large-scale variables. In this analysis, to avoid issues of non stationarity and GCM bias, both predictors and predictands are first converted to anomalies (the differences between the monthly means and standard deviations and their long-term (1958–2001) averages). The variability of the suite of potential predictors from the GCM simulations was then evaluated relative to the reanalysis data. Following the approach of Chervin (1981) and Portman *et al*. (1992), 100 expanded data sets, each containing 12 randomly chosen years,

Table II. Upper-atmosphere and surface predictor variables and examples of their use in previous temperature downscaling studies

Predictor (units)	Abbrev.	Previous studies
Upper-atmosphere variables		
850 hPa geopotential height (m)	Z_{850}	Sailor and Li, 1999
500 hPa geopotential height (m)	Z_{500}	Weichert and Burger, 1998
–	–	Sailor and Li, 1999
–	–	Palutikof *et al*., 2002
–	–	Huth, 2004
850–500 hPa thickness (m)	THICK	Kidson and Thompson, 1998
850 hPa specific humidity (kg/kg)	Q_{850}	Murphy, 1999
850 hPa relative humidity (%)	RH_{850}	Sailor and Li, 1999
Surface variables		
Mean sea-level pressure (hPa)	SLP	Schubert, 1998
–	–	Palutikof *et al*., 2002
–	–	Kettle and Thompson, 2004
–	–	Frias *et al*., 2005
Zonal component of geostrophic flow (hPa/10° latitude at grid cell latitude)	GEOW	Buishand and Brandsma, 1997 Kidson and Thompson, 1998
Meridional component of geostrophic flow (hPa/10° latitude at grid cell latitude)	GEOS	–
Strength of the resultant geostrophic flow (hPa/10° latitude at grid cell latitude)	GEOWS	–
Westerly shear vorticity (hPa/10° latitude at grid cell latitude, per 10° latitude)	GEOZW	–
Southerly shear vorticity (hPa/10° latitude at grid cell latitude, per 10° latitude)	GEOZS	–
Total shear vorticity (hPa/10° latitude at grid cell latitude, per 10° latitude)	GEOZT	

DOI: 10.1002/joc

are constructed from the reanalysis data (1958–2001) and compared to the 12 years of GCM output. It should be noted that the output of 12 years represents a relatively small amount of data for model evaluation and precludes the analysis of grid cell GCM data at higher (e.g. daily) time steps. This 12-year evaluation period is dictated by the short period of overlap between the daily transient GCM and reanalysis data (1990–2001).

Comparison of the 1990–2001 GCM simulations with the 1958–2001 reanalysis data is based on the assumption that the 1958–2001 reanalysis data are also representatives of the 1990–2001 period. To test this assumption, the methodology described above was also applied to test the agreement between the 1990–2001 and 1958–2001 reanalysis data sets. For each variable and grid point, we were unable to reject the null hypothesis of equal variances.

For each GCM and variable, an F-test is performed to test the null hypothesis that the anomalies computed at the monthly timescale from reanalysis data and GCM simulations have equal variances. These tests were performed on the monthly anomalies for each variable in Table II at each of the GCM grid cells nearest to the downscaling stations (23 unique grid cells, see Figure 1). This null hypothesis can be rejected if a sufficient number of tests fail (e.g. 95 rejections out of 100 tests with $\alpha = 0.05$). The results indicate that HadCM3 and CGCM2 differ considerably in their ability to reproduce the variability present in the observed (reanalysis) anomaly series. With the exception of the resultant geostrophic wind speed and geostrophic vorticity variables, the null hypotheses of equal reanalysis and HadCM3 variances cannot be rejected at the majority of grid points (Table III). For each of the three geostrophic vorticity variables, the null hypothesis of equal variances is rejected at each grid point, precluding these variables from use in the statistical models. Tests performed on CGCM2 resulted in fewer rejections of the null hypothesis for the vorticity variables, but a greater overall number of significantly different reanalysis and GCM variances (Table III). For CGCM2, the resultant geostrophic wind speed, 500-hPa height, 850-hPa specific humidity, and 850–500 hPa thickness are all found to have significantly different variances at each grid point tested, while the null hypotheses for the remaining variables are rejected at a smaller number of grid points.

Results of this evaluation suggest that, for the current climate, anomalies of some of the GCM predictor variables are not consistent with reanalysis data sets. To address this issue, in the downscaling analysis we use only the variables for which the null hypothesis of equal variances was not rejected. This approach, combined with the use of anomalies, ensures that the downscaling equations built with reanalysis data can be meaningfully applied to the GCM simulations. The downscaling is thus optimized for each station and because grid cell variables are used only if they exhibit agreement with reanalysis data slightly different combinations of predictor variables are used for different stations and predictands.

Table III. Results of hypothesis tests on the equality of variances between anomalies computed from the reanalysis data and GCM simulations during the period of overlap (1990–2001). Values represent the number of grid cells (out of the 23 reanalysis grid cells used in this study) where the null hypothesis of equal variances is rejected (with $\alpha = 0.05$)

Variable	HadCM3	CGCM2
GEOS	0	16
GEOW	0	0
GEOWS	14	23
GEOZS	23	5
GEOZW	23	6
GEOZT	23	3
Z_{500}	0	23
Z_{850}	0	8
RH_{850}/Q_{850}	2	23
SLP	0	0
THICK	2	23

For each seasonal cycle (the daily means and standard deviations of T_{max} and T_{min}), the regression models are built in a stepwise fashion, with variables added until the improvement in variance explained is less than 5%. This threshold was used to provide a high level of variance explained without overfitting the model. The variables included in the final models for the seasonal cycles and correlation coefficients are shown in Tables IV and V, respectively. These tables not only provide a synopsis indicating which variables are closely linked to the predictands within the observed record, but also reflect the ability of the GCMs to reproduce the variability of each predictor. The values in the tables indicate that, in general, both models are using similar predictors. For example, for the mean temperatures, both models primarily use geopotential heights and sea-level pressure. This result suggests that differences in the downscaled data are likely to result from model differences rather than differences in the downscaling predictors.

The resulting regression equations are applied to HadCM3 and CGCM2 output from 1990–2001, 2020–2029, and 2050–2059 to produce station-specific time series of the monthly anomalies of T_{max} and T_{min} for each GCM and period. The anomalies are then averaged over each calendar month and added to the observed monthly means and standard deviations of daily T_{max} and T_{min} to produce monthly values consistent with the GCM simulations. In order to produce the 365 daily values needed to apply the weather generator, cubic splines were used to interpolate the monthly values resulting in daily values of the means and standard deviations of T_{max} and T_{min}. An example of the downscaled seasonal cycles is shown in Figure 2.

DOI: 10.1002/joc

Table IV. List of variables used in final models for downscaling the seasonal cycles of T_{max} and T_{min}. The downscaling is performed at 26 stations. The number indicates the number of stations at which each variable was used. For each GCM, information is provided for the downscaling of the mean T_{max} (MT_{max}), mean T_{min} (MT_{min}), standard deviation of T_{max} (ST_{max}) and standard deviation of T_{min} (ST_{min}). The variables are as shown in Table II. An 'M' preceding the predictor variable name indicates that the mean was used, while an 'S' indicates that the standard deviation was used

Predictor Variable	HadCM3				CGCM2			
	MT_{max}	MT_{min}	ST_{max}	ST_{min}	MT_{max}	MT_{min}	ST_{max}	ST_{min}
MGEOS	–	3	–	–	–	–	3	–
MGEOW	3	–	–	–	–	–	6	5
MGEOWS	–	–	–	–	–	–	–	–
MGEOZS	–	–	–	–	–	–	–	–
MGEOZW	–	–	–	–	–	–	–	–
MGEOZT	–	–	–	–	–	–	–	–
MZ_{500}	3	3	14	2	6	8	–	–
MZ_{850}	23	22	–	1	18	19	1	1
MRH_{850}/MQ_{850}	–	1	–	–	–	–	–	–
MSLP	23	22	–	5	23	25	–	19
MTHICK	–	1	1	–	7	3	–	–
SGEOS	–	–	–	1	–	–	1	3
SGEOW	–	–	7	–	–	–	3	–
SGEOWS	–	–	–	–	–	–	–	–
SGEOZS	–	–	–	–	–	–	–	–
SGEOZW	–	–	–	–	–	–	–	–
SGEOZT	–	–	–	–	–	–	2	1
SZ_{500}	–	–	3	5	–	–	–	–
SZ_{850}	–	–	2	3	–	–	3	5
SRH_{850}/SQ_{850}	–	–	–	–	–	–	–	–
SSLP	–	–	2	3	–	–	11	18
STHICK	–	–	23	21	–	–	–	

Downscaling of the lag-0 and lag-1 correlation coefficients

Variability in the lag-0 and lag-1 correlation matrices used in the WGEN model is physically linked to variations in large-scale circulation through persistence of synoptic-scale systems and the subsequent effect on temperatures at the station level. To develop models for the correlation coefficients, we examine relationships between monthly correlation coefficients and monthly means and standard deviations of the predictors as manifest in the NCEP/NCAR and ECMWF reanalysis products using data from 1958–2001 (44 years of data at the monthly time scale, so $n = 528$). As with the seasonal-cycle downscaling described above, we develop and apply the models using anomalies and then use these anomalies to reconstruct new monthly values from the GCM simulations. Cubic splines are then used with the monthly values to derive daily values of the parameters. A scatterplot depicting an example of the observed and downscaled values of $M_0(1, 2)$ (the unique element of the lag-0 cross-correlation matrix) is shown in Figure 3 and indicates the overall agreement achieved by this methodology.

The weather generator

WGEN generates T_{max} and T_{min} with a first order multiple autoregressive model, first described by Matalas (1967):

$$X_i = A_i X_{i-1} + B_i \varepsilon_i \tag{1}$$

where X_i is a matrix containing the current day's standardized values of the variables and X_{i-1} is a matrix containing the previous day's standardized values of the variables, ε_i is a vector of independent values from a standard normal distribution, and A and B are matrices given by

$$A = M_1 M_0^{-1} \tag{2}$$

$$BB^T = M_0 - M_1 M_0^{-1} M_1^T \tag{3}$$

where M_0 is the matrix of lag-0 cross correlations and M_1 is the matrix of lag-1 cross correlations. The subscripts in (1) reflect that A and B are allowed to vary throughout the course of the year. While A can be directly computed, B is computed by defining a new matrix $Z = BB^T$ (see Greene, 2000). Then $Z = CLC^T$, where C is the matrix of eigenvectors of BB^T and L has the eigenvalues of BB^T on the diagonal and zeros elsewhere. B can then be computed as $B = CL^{1/2}C^T$. After generation of the residual series with (1), dimensional values of the variables are produced by multiplying by a daily standard deviation and then adding a daily mean. These daily means and standard deviations are usually derived by

DOI: 10.1002/joc

Table V. List of variables used in final models for downscaling the lag-0 and lag-1 correlations between T_{max} and T_{min}. The downscaling is performed at 26 stations. The number indicates the number of stations at which each variable was used. For each GCM, information is provided for the downscaling of the lag-0 correlation between T_{max} and T_{min} (M_0 (1,1)), the lag-1 correlation of T_{max} ($M_1(1, 1)$), the lag-1 correlation between T_{max} and T_{min} ($M_1(1, 2)$), the lag-1 correlation between T_{min} and T_{max} ($M_1(2, 1)$) and the lag-1 correlation of T_{min} ($M_1(2, 2)$). An 'M' preceding the predictor variable name indicates that the mean was used, while an 'S' indicates that the standard deviation was used

Predictor Variable	HadCM3					CGCM2				
	$M_0(1, 1)$	$M_1(1, 1)$	$M_1(1, 2)$	$M_1(2, 1)$	$M_1(2, 2)$	$M_0(1, 1)$	$M_1(1, 1)$	$M_1(1, 2)$	$M_1(2, 1)$	$M_1(2, 2)$
MGEOS	–	–	–	–	–	–	–	3	1	2
MGEOW	–	3	–	–	1	4	–	1	2	–
MGEOWS	–	–	–	–	–	–	–	–	–	–
MGEOZS	–	–	–	–	–	–	–	2	1	–
MGEOZW	–	–	–	–	–	–	–	–	–	–
MGEOZT	–	–	–	–	–	–	1	1	1	–
MZ_{500}	5	–	10	–	6	1	3	3	11	5
MZ_{850}	7	9	5	5	16	6	1	6	5	15
MRH_{850}/MQ_{850}	–	–	–	–	3	–	–	–	–	–
MSLP	–	–	–	–	–	8	10	6	6	6
MTHICK	–	–	–	–	–	–	3	–	7	1
SGEOS	–	1	–	–	–	3	–	1	–	–
SGEOW	–	–	–	–	–	1	2	–	–	–
SGEOWS	–	–	–	–	–	–	–	–	–	–
SGEOZS	–	–	–	–	–	1	3	1	3	1
SGEOZW	–	–	–	–	–	–	2	1	1	1
SGEOZT	–	–	–	–	–	–	5	1	2	–
SZ_{500}	2	15	2	2	2	–	–	–	–	–
SZ_{850}	2	–	2	–	–	3	3	3	–	–
SRH_{850}/SQ_{850}	–	1	3	2	1	–	–	–	–	–
SSLP	2	–	2	–		9	1	7	4	1
STHICK	24	11	23	24	24	–	–	–	–	

fitting smooth curves to the observed daily means and standard deviations. In the application presented here, the downscaled values of MO and M1 are used to compute A and B. Equation 1 is then used with the downscaled daily means and standard deviations to produce data series consistent with the climate change signal implied by the GCMs.

Comparison with a common downscaling method

As stated in the introduction, many downscaling methods are based on transfer-function methodologies. Typically, a relationship is established between observed large-scale and surface variables and then applied to GCM output to derive the downscaled surface climate. Thus, such methods assume that the GCM adequately simulates the predictor variables upon which the downscaling is based. However, this assumption is rarely tested in practice. Note that the approach used here to downscale the seasonal cycles and lag-0 and lag-1 correlation coefficients is less susceptible to such problems, since the methodology uses anomalies and removes variables that are shown to have inadequate variability within the GCM.

To provide a context for the new hybrid downscaling approach, we compare the 1990–2001 results with those from a traditional downscaling method based on monthly transfer functions derived from regression analysis of the 1958–2001 reanalysis data and the surface temperature data. Specifically, monthly regression models are built using the 1958–2001 observations and then applied to the 1990–2001 GCM output for comparison with the results produced by the weather generator with downscaled parameters. As with the seasonal-cycle downscaling, variables are added until the variance explained decreases by less than 5% and only the variables that are adequately simulated by the GCMs are allowed to enter the regression equations.

An example of the results from the methodological comparison is shown in Figure 4 and indicates that the downscaling approach based on weather generation techniques produces results that have better agreement with observations. For the station depicted in Figure 4 (Princeton, IN), the results indicate an improvement in agreement for both the monthly means and standard deviations. Results from other stations are similar, although downscaling using the weather generator generally results in greater improvement for the standard deviations of T_{max} and T_{min} than their means. Previous studies have indicated substantial underestimation of variance in statistically downscaled data (see von Storch, 1999). It is noteworthy that the method presented here does not require the use of variance inflation techniques.

DOI: 10.1002/joc

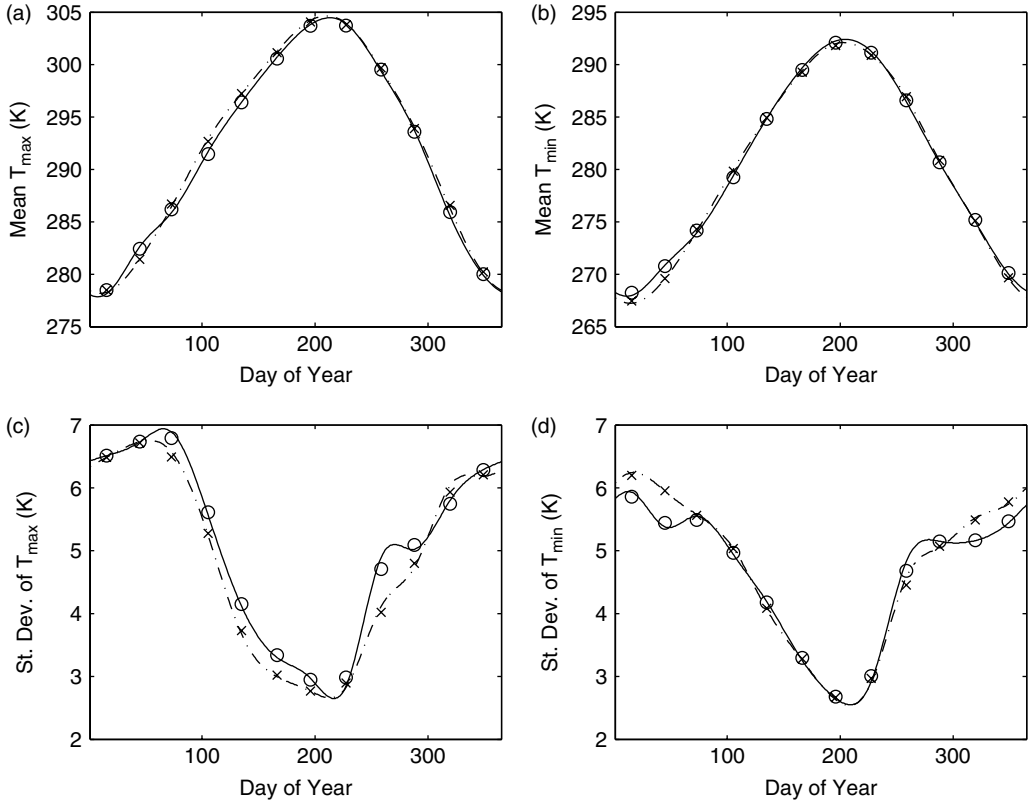

Figure 2. An example of the seasonal-cycle downscaling applied to CGCM2 output and Mountain Grove, MO, for the period 1990–2001. The solid line represents the observed values, and the observed monthly means are also shown (○). The downscaled monthly means are depicted by '×', with the dashed line showing the daily values (from cubic spline interpolation of the monthly means): (a) mean T_{max}, (b) mean T_{min}, (c) standard deviation of T_{max}, and (d) standard deviation of T_{min}

RESULTS

Projected changes in temperature means and variances

The projected changes in daily T_{max} and T_{min} for 2020–2029 relative to 1990–2001 differ substantially between the two GCMs (see Figures 5 and 6). Specifically, downscaled results from HadCM3 indicate slight cooling at most, but not all, stations during the winter and spring, moderate warming during summer, and slight, but consistent, warming during autumn (Figure 5). On an annual basis, this equates to a warming of 0.0–0.5 K at most stations (Figure 6). Although direct output from HadCM3 (taken as the value at the grid point nearest the station) indicates slight warming in T_{max} (<1.0 K) at most grid cells, two stations in the northeast part of the domain exhibit lower temperatures in the 2020s than during the 1990–2001 reference period (Figure 7(b)). Direct T_{min} output from HadCM3 indicates cooling over approximately 1/3 of the study area (Figure 7(d)). Direct output from CGCM2 shows a slightly larger increase in both T_{max} and T_{min} relative to the downscaled data (compare Figure 6 and Figure 7).

Downscaled results from CGCM2 indicate year-round warming in both T_{max} and T_{min}, with the weakest warming during spring and largest increases during autumn and winter (see Figures 5 and 6). Annually, downscaled projections from CGCM2 indicate T_{max} and T_{min} increases of 0.5–2 K (Figure 6). The largest differences in the downscaled GCM projections are associated with winter temperatures (Figure 5). Examination of results from individual stations shows that although the magnitude of temperature changes exhibited by HadCM3 and CGCM2 during summer is similar, HadCM3 results indicate greater warming at stations in the central part of the domain (primarily those in Indiana and Ohio). During autumn, the spatial patterns of warming exhibit general agreement, although the magnitude of warming is considerably larger in the results downscaled from CGCM2. Temperature changes computed over the entire year exhibit only small amounts of spatial variability and hence the differences in spatial variability are difficult to assess (Figure 6). With respect to temperature variability, the results from both GCM experiments imply only small changes in the standard deviation of daily air temperature (<0.5 K). However, the relationship between changes in the mean and variance also differ between models. CGCM2 shows a weak negative variance response to increases in mean temperatures, which is consistent with previous studies (e.g. Robeson, 2002). HadCM3 exhibits an overwhelmingly positive variance response. The correlation between monthly changes in the mean and standard deviation (over all the stations) is −0.20 for CGCM2 and 0.57 for HadCM3.

As expected, the projected changes in daily T_{max} and T_{min} for 2050–2059 are larger than those for 2020–2029

DOI: 10.1002/joc

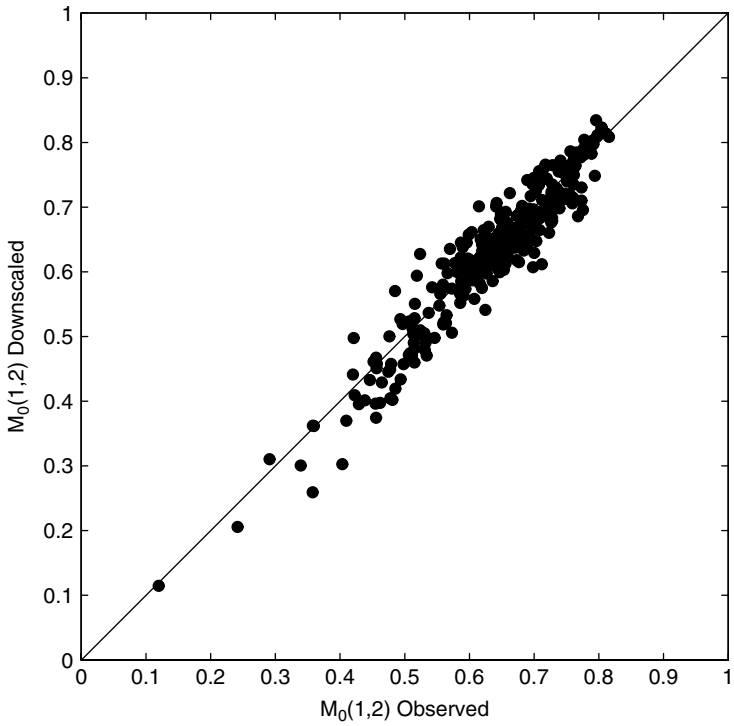

Figure 3. Scatter diagram showing observed and CGCM2-downscaled values of the lag-0 correlation between T_{max} and T_{min} ($M_0(1, 2)$). Each dot represents one station and one month

(compare Figures 5 and 8 and the frames in Figure 6). The accelerated warming suggested by these results may be due to the increased rate of CO_2 accumulation by the middle of the 21st century, as specified by the SRES A2 scenario. The seasonal characteristics of projected temperature changes also differ from the 2020–2029 period. Temperatures downscaled from HadCM3 exhibit the smallest increase during spring, while those downscaled from CGCM2 show the smallest increase during summer (Figure 8). Although results downscaled from both models indicate year-round warming for the period 2050–2059 relative to the present day, and similar annual temperature increases at most stations (Figure 6), the magnitude and seasonality of the warming differs considerably and is larger in results downscaled from CGCM2 output, with the exception of summer (Figure 8). Results from both GCMs exhibit a weak negative variance response overall, with some stations exhibiting increases in variability and others exhibiting decreases.

The downscaled seasonal cycles of T_{max} and T_{min} from both GCMs indicate warming at most stations, consistent with recent observations and the increases in greenhouse gases on which the model projections are based. However, the results from the models are substantially different from each other, and temperatures downscaled from HadCM3 are inconsistent with the trends in recent observations (e.g. Folland *et al*., 2001), specifically during the winter season. It is noteworthy that there are differences in the downscaled projections for nearby stations, which lie within the same GCM grid cell (often >0.5 K, see Figures 6 and 7). This may reflect local environmental factors that influence the station data, but are not accounted for in the coarse-resolution GCM data.

Projected changes in lag-0 and lag-1 correlation coefficients

When applied to HadCM3 and CGCM2 projections for 2020–2029 and 2050–2059, the regression equations used to downscale the lag-0 and lag-1 correlations between T_{max} and T_{min} result in only minor changes in monthly statistics, indicating little change in the relationship between T_{max} and T_{min}, which is consistent with recent studies (e.g. Vose *et al*., 2005). In general, projected changes in the elements of both M_0 and M_1 are less than $|0.05|$. Projection changes of the elements of both M_0 and M_1 are less than $|0.1|$ for all stations and all months for both future periods. This result provides some justification for previous studies, such as that of Qian *et al*. (2005), which assumed no changes in M_0 and M_1 for a weather generator applied to climate change simulations. To produce climate change scenarios as consistent as possible with the GCM simulations, we use these slightly changed values of M_0 and M_1.

Projected changes in extreme events

Prolonged periods of extreme high temperatures have received increased attention in recent years owing to their impact on human mortality. The weather generator was thus used to generate a 100-year sequence consistent with the climate change signal to allow probability-based estimates of changes in the frequency of extreme events. Prior to examining future changes, we considered the performance of the downscaled data relative to

DOI: 10.1002/joc

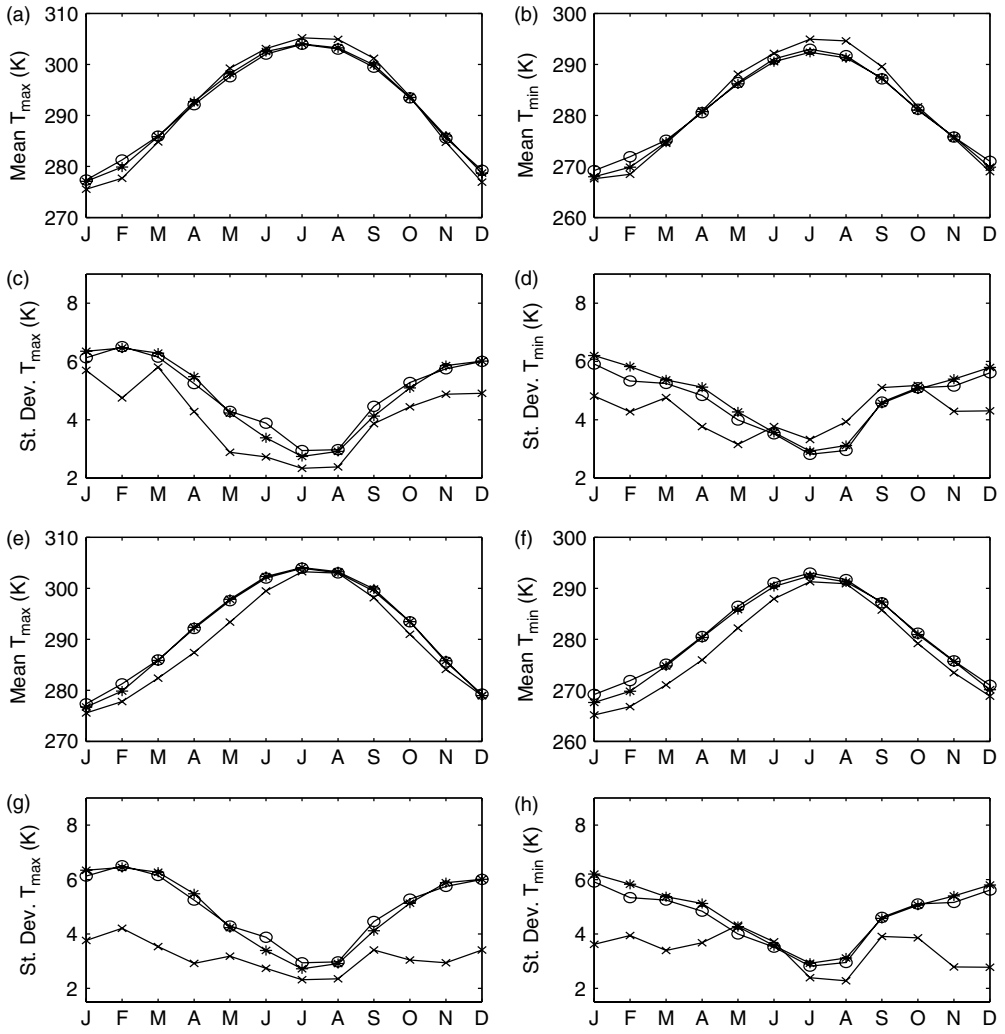

Figure 4. Comparison of results obtained by downscaling weather-generator parameters and a simple transfer-function methodology. Monthly means and standard deviations are shown for a single station (Princeton, IN) for the period 1990–2001. For each month, three symbols are used: observed data (○), data predicted using downscaled weather-generator parameters (*), and data predicted using a regression-based transfer function (×). The individual panels depict results from: (a) HadCM3 T_{max} mean, (b) HadCM3 T_{min} mean, (c) HadCM3 T_{max} standard deviation, (d) HadCM3 T_{min} standard deviation, (e) CGCM2 T_{max} mean, (f) CGCM2 T_{min} mean, (g) CGCM2 T_{max} standard deviation, and (h) CGCM2 T_{min} standard deviation

observations over the 1990–2001 period. During this period, the data downscaled from both GCMs tends to produce extreme warm days too infrequently. Averaged over all stations, the 95th percentiles of T_{max} and T_{min} differ from observed values by 0.6–0.7 K and 1.3–1.4 K, respectively. On the basis of this finding, we present our results in terms of differences between heat waves in the current and future downscaled GCM climates, rather than comparing the downscaled future GCM climate with current observations.

There is no standard definition of a heat wave (Robinson, 2001; Souch and Grimmond, 2004). For the purposes of this study, we define a heat wave as a period of at least three days in which T_{max} and T_{min} both remain above their respective 97.5th percentiles (defined using the 1958–2001 surface data). The percentile-based definition is used here rather than fixed thresholds because previous work has suggested that such thresholds should be location specific (e.g. Kalkstein and Davis, 1989; Smoyer *et al*., 2000; Watts and Kalkstein, 2004). The number of heat waves in both the current and downscaled climates will be dependent on this choice of definition. We analyze occurrence of 3-, 4-, and 5-day heat waves in the observed record (1958–2001) and in the stochastically generated GCM downscaled series for 1990–2001, 2020–2029, and 2050–2059. Although longer heat waves have occurred in the past at the stations analyzed here, they are extremely rare events.

The results, summarized in Figure 9, indicate an increase in the occurrence of heat waves in the series downscaled from both GCMs. While CGCM2 indicates only minor increases in heat wave occurrence by the 2020s, temperatures downscaled from HadCM3 indicate an increase of more than 4 three-day heat waves per decade. This result is consistent with the increase in the variability of summer temperatures downscaled from HadCM3. For the 2050s, the results show less disparity, with downscaled results indicating an increase of around

DOI: 10.1002/joc

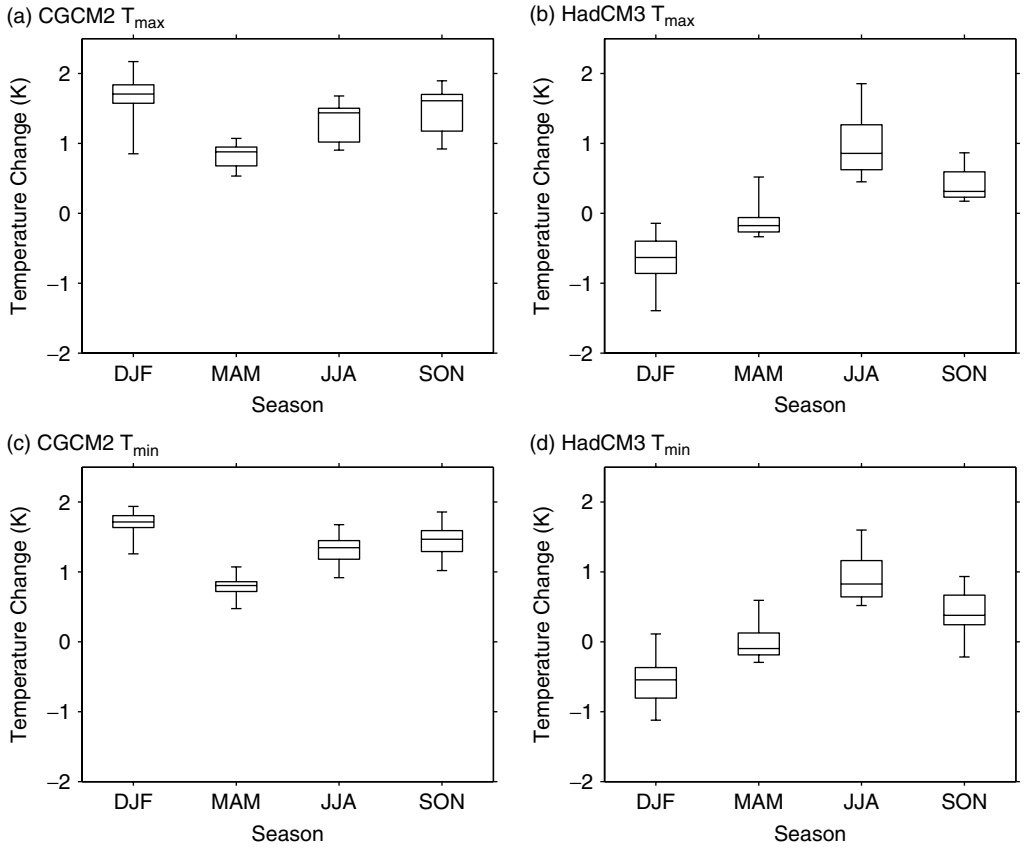

Figure 5. Box-and-whisker plots of seasonal temperature change projections from downscaled CGCM2 and HadCM3 output. The y-axis indicates temperature change for 2020–2029 relative to 1990–2001. The ends of the whiskers indicate the maximum and minimum values (across stations), while the height of the box indicates the inter-quartile range. The line in the middle of each box represents the median. Spatial variability can be inferred from the height of the box and whiskers. Results are shown for (a) CGCM2 T_{max}, (b) HadCM3 T_{max}, (c) CGCM2 T_{min}, and (d) HadCM3 T_{min}, and synthesize the changes in temperatures across all 26 stations

17 and 11 three-day heat waves per decade from HadCM3 and CGCM2, respectively (Figure 9). These results can be attributed to the larger increase in summer temperatures downscaled from HadCM3 relative to CGCM2 for the 2050s. The changes in heat wave occurrence from both models are largest at southern stations. The increases discussed above are particularly large given the relative rarity of such events in the 1990–2001 simulations. Averaged over all stations, three-day heat waves during the 1990–2001 period occur at a rate of 0.7 events per decade and 0.03 events per decade for HadCM3 and CGCM2, respectively. Recent heat waves have occurred in both Chicago (Changnon *et al*., 1996) and St Louis (Smoyer, 1998). Examination of results from nearby stations (Jacksonville, IL and LaPorte, IN) suggests that heat waves will become more frequent at both locations, although the increase in frequency is greater at the station near St Louis (Figure 10). In accord with results averaged over all stations, larger increases are indicated from the results downscaled from HadCM3.

Both Schar *et al*. (2004) and Meehl and Tebaldi (2004) report a potential increase in future heat waves over Europe owing to increases in interannual variability of surface temperatures. While the results presented in this study do not address interannual temperature variations, the downscaled results indicate an increase in the number of heat waves due to an increase in variability for the 2020s, but an increase in heat waves in the absence of a widening of the daily temperature probability distribution for the 2050s.

CONCLUSIONS

In this study, we have developed and applied a new hybrid downscaling methodology based on regression analysis of weather-generator parameters. The parameters downscaled from 1990–2001, 2020–2029, and 2050–2059 GCM simulations were then used to stochastically generate data for these periods at 26 stations in the Midwestern USA. Results for the reference period (1990–2001) showed that the new methodology produces results that exhibit better agreement with observations than a traditional transfer-function method, especially with respect to temperature variability.

The downscaled seasonal cycles of T_{max} and T_{min} from both GCMs indicate warming at most stations, which is consistent with recent observations and the increases in greenhouse gases on which the model projections are based. The results from the two GCMs, however, are substantially different on a seasonal basis,

DOI: 10.1002/joc

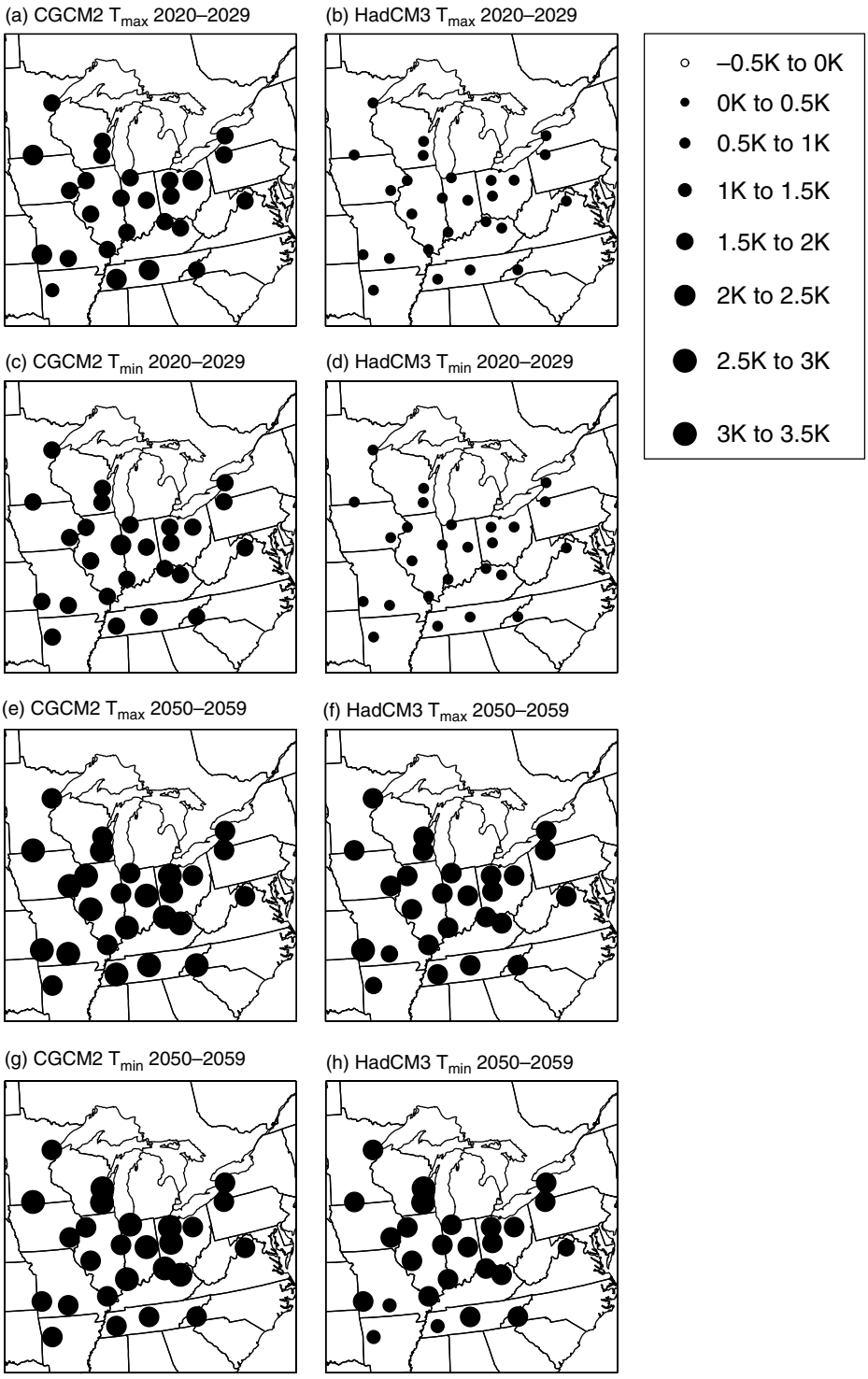

Figure 6. Projected changes in annual mean T_{max} and T_{min} based on downscaled GCM output for (a) CGCM2 T_{max} 2020–2029, (b) HadCM3 T_{max} 2020–2029, (c) CGCM2 T_{min} 2020–2029, (d) HadCM3 T_{min} 2020–2029, (e) CGCM2 T_{max} 2050–2059, (f) HadCM3 T_{max} 2050–2059, (g) CGCM2 T_{min} 2050–2059, and (h) HadCM3 T_{min} 2050–2059. The maps depict changes from 1990–2001 values

resulting in lowered confidence regarding the downscaled results.

Results from the stochastically generated temperature scenarios also indicate increases in heat wave occurrence. However, while the results downscaled from HadCM3 and CGCM2 both indicate increases in heat wave occurrence, the details of the increases differ, with HadCM3 projecting a much larger increase in heat wave occurrence than CGCM2. For the 2020s, the additional heat waves are primarily due to increases in the variability of daily temperatures. For the 2050s, however, the additional heat waves result from large increases in summer temperatures.

The downscaling methods presented here are capable of reproducing the major features of the observed climate over the period in which station observations and GCM

DOI: 10.1002/joc

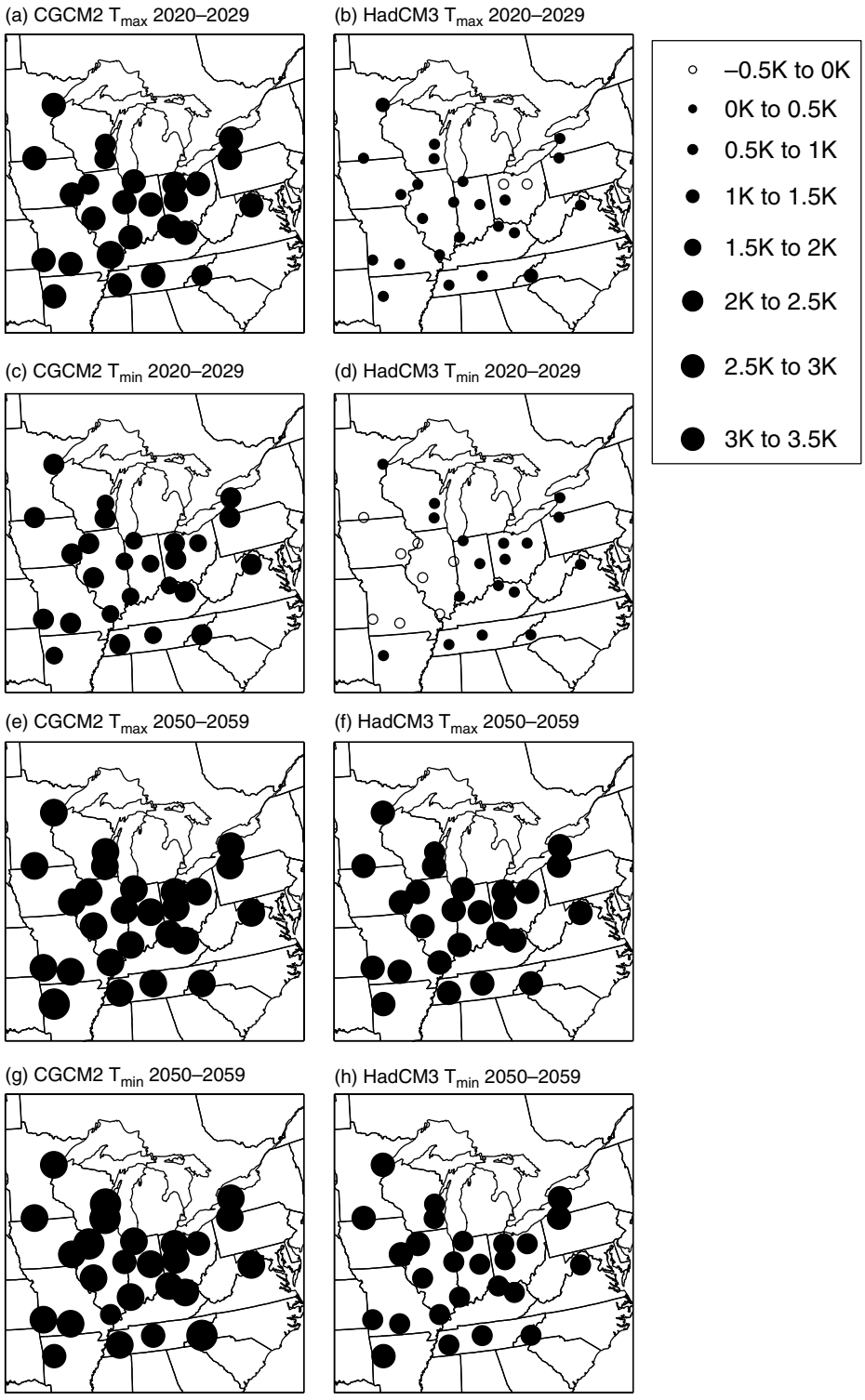

Figure 7. Projected changes in annual mean T_{max} and T_{min} based on direct GCM output for (a) CGCM2 T_{max} 2020–2029, (b) HadCM3 T_{max} 2020–2029, (c) CGCM2 T_{min} 2020–2029, (d) HadCM3 T_{min} 2020–2029, (e) CGCM2 T_{max} 2050–2059, (f) HadCM3 T_{max} 2050–2059, (g) CGCM2 T_{min} 2050–2059, and (h) HadCM3 T_{min} 2050–2059. The maps depict changes from 1990–2001 values

simulations coexist (1990–2001). However, although the downscaling was conducted using GCMs with identical forcing scenarios and downscaling methodologies and similar predictor variables, the resulting temperature scenarios exhibited large discrepancies. Future work will address these issues by focusing on identifying physical causes for these differences and expanding the work presented here to include systematic evaluation of other GCMs using identical sets of predictor variables. Future work will also incorporate a longer period of overlap between the observed data and GCM simulations to allow investigation of interannual variability. Although these differences demonstrate the uncertainty of GCM-based regional climate downscaling, the improvement

DOI: 10.1002/joc

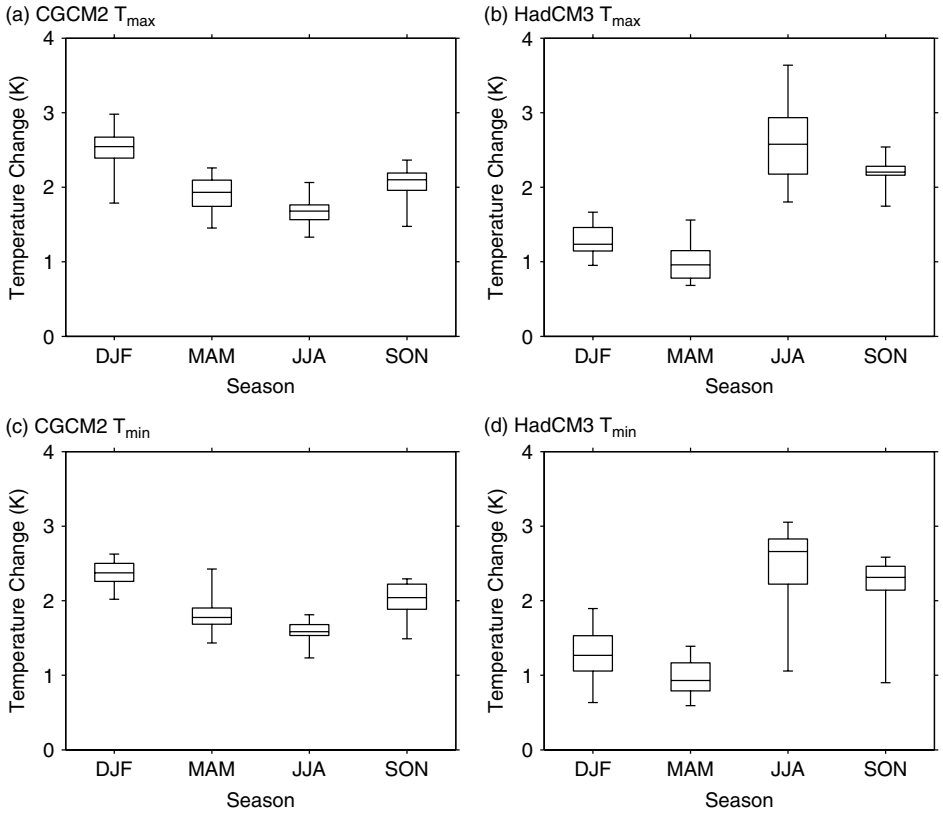

Figure 8. Same as in Figure 5, but for 2050–2059

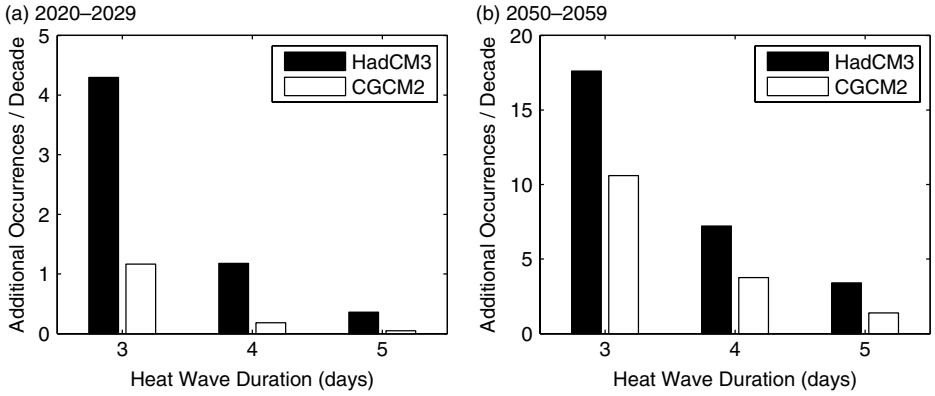

Figure 9. Projected increases in heat wave occurrence averaged over all stations resulting from downscaled HadCM3 and CGCM2 output for (a) 2020–2029 and (b) 2050–2059

obtained by applying these new innovative downscaling methods to multiple GCMs should increase confidence in the projected magnitude and potential impacts of future warming at the regional scale.

REFERENCES

Bardossy A, Stehlik J, Caspary H-J. 2002. Automated objective classification of daily circulation patterns for precipitation and temperature downscaling based on optimized fuzzy rules. *Climate Research* **23**: 11–22.

Bellone E, Hughes JP, Guttorp P. 2000. A hidden Markov model for downscaling synoptic atmospheric patterns to precipitation amounts. *Climate Research* **15**: 1–12.

Buishand TA, Brandsma T. 1997. Comparison of circulation classification schemes for predicting temperature and precipitation in The Netherlands. *International Journal of Climatology* **17**: 875–889.

Changnon SA, Kunkel KE, Reinke BC. 1996. Impacts and responses to the 1995 heat wave: a call to action. *Bulletin of the American Meteorological Society* **77**: 1497–1506.

Chervin RM. 1981. On the comparison of observed and GCM simulated climate ensembles. *Journal of the Atmospheric Sciences* **38**: 885–901.

Cubasch U, Meehl GA, Boer GJ, Stouffer RJ, Dix M, Noda A, Senior CA, Raper S, Yap KS. 2001. Projections of Climate Change. In *Climate Change 2001: The Scientific Basis. Contribution of Working Group I to the Third Assessment Report of the Intergovernmental Panel on Climate Change*, Houghton JT, Ding Y, Griggs DJ, Noguer M, van der Linden PJ, Dai X, Maskell K (eds). Cambridge University Press: Cambridge, New York, USA; 881.

Dessouky TM, Jenkinson AF. 1975. An objective daily catalogue of surface pressure, flow, and vorticity indices for Egypt and it's use in monthly rainfall forecasting. *Meteorological Research Bulleting, Egypt* **11**: 1–25.

DOI: 10.1002/joc

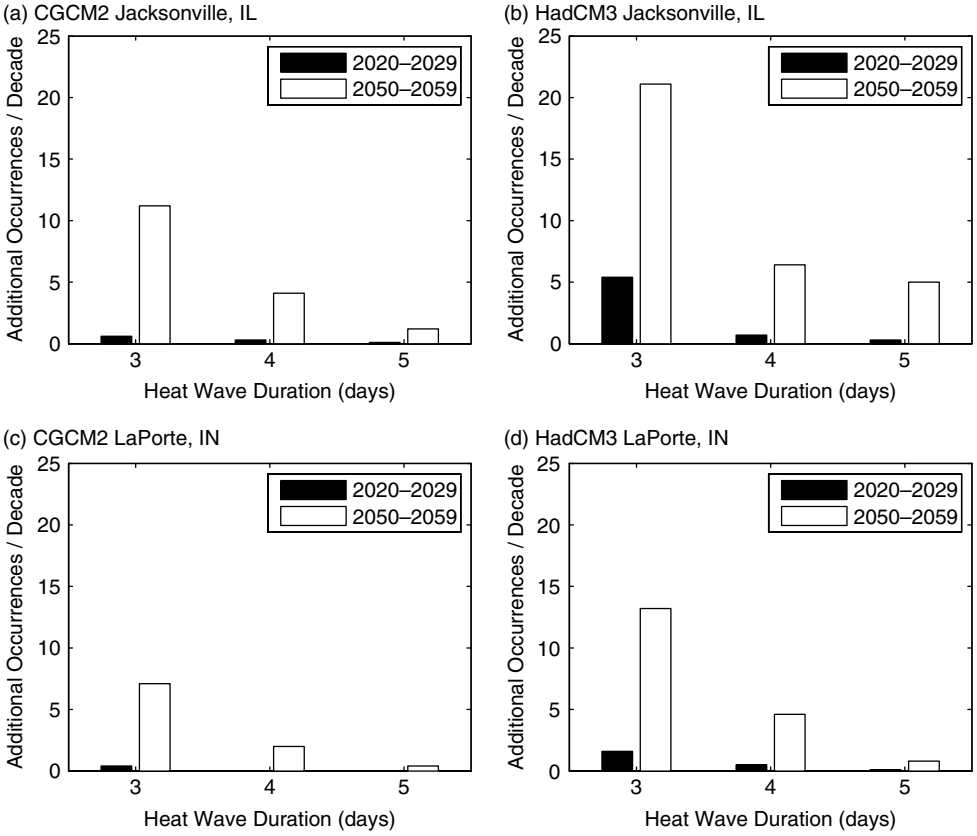

Figure 10. Projected increases in heat wave occurrence in 2020–2029 and 2050–2059 relative to 1990–2001 at stations near St Louis, MO (Jacksonville, IL) and Chicago, IL (LaPorte, IN). Results are shown for CGCM2 (left column) and HadCM3 (right column)

Easterling DR, Karl TR, Lawrimore JH, Del Greco SA. 1999. *United States Historical Climatology Network Daily Temperature, Precipitation, and Snow Data for 1871–1997*. Oak Ridge National Laboratory: Oak Ridge, TN; 84.

Flato GM, Boer GJ. 2001. Warming asymmetry in climate change simulations. *Geophysical Research Letters* **28**: 195–198.

Flato G, Boer GJ, Lee WG, McFarlane NA, Ramsden D, Reader MC, Weaver AJ. 2000. The Canadian Centre for Climate Modelling and Analysis global coupled model and its climate. *Climate Dynamics* **16**: 451–467.

Folland CK, Karl TR, Christy JR, Clarke RA, Gruza GV, Jouzel J, Mann ME, Oerlemans J, Salinger J, Wang S-W. 2001. Observed Climate Variability and Change. In *Climate Change 2001: The Scientific Basis. Contribution of Working Group I to the Third Assessment Report on the Intergovernmental Panel on Climate Change*, Houghton JT, Ding Y, Griggs DJ, Johnson CA (eds). Cambridge University Press: Cambridge, New York, USA; 881.

Frias MD, Fernandez J, Saenz J, Rodriguez-Puebla C. 2005. Operational predictability of monthly average maximum temperature over the Iberian Peninsula using DEMETER simulations and downscaling. *Tellus* **57A**: 448–463.

Gibson JK, Kallberg P, Uppala S, Noumura A, Hernandez A, Serrano E. 1997. *ERA Description*. ECMWF Reanalysis Project Report Series: Reading.

Giorgi F, Hewitson BC, Christensen J, Hulme M, von Storch H, Whetton P, Jones R, Mearns L, Fu C. 2001. Regional climate information – evaluation and projections. In *Climate Change 2001: The Scientific Basis. Contribution of Working Group i to the Third Assessment Report of the Intergovernmental Panel on Climate Change*, Houghton JT, Ding Y, Griggs DJ, Noguer M, van der Linden PJ (eds). Cambridge University Press: Cambridge, New York, USA; 881.

Goodess CM, Palutikof JP. 1998. Development of daily rainfall scenarios for Southeast Spain using a circulation-type approach to downscaling. *International Journal of Climatology* **10**: 1051–1083.

Gordon C, Cooper C, Senior CA, Banks H, Gregory JM, Johns TC, Mitchell JFB, Wood RA. 2000. The simulation of SST, sea ice extents and ocean heat transports in a version of the Hadley Centre coupled model without flux adjustments. *Climate Dynamics* **16**: 147–168.

Greene WH. 2000. *Econometric Analysis*. Prentice Hall: Upper Saddle River, NJ.

Hansen J, Lacis A, Rind D, Russell G 1984. Climate sensitivity: Analysis of feedback mechanisms. *Climate Processes and Climate Sensitivity, Geophysical Monographs 29.* American Geophysical Union; 130–163.

Huth R. 2004. Sensitivity of local daily temperature change estimates to the selection of downscaling models and predictors. *Journal of Climate* **17**: 640–652.

IPCC. 2000. *Special Report on Emissions Scenarios*. Cambridge University Press: Cambridge; 612.

Jenkinson AF, Collison P. 1977. *An Initial Climatology of Gales Over the North Sea*. Meteorological Office: London; 18.

Jones PD. 1994. Hemispheric surface air temperature variations: a reanalysis and an update to 1993. *Journal of Climate* **7**: 1794–1802.

Jones PD, Hulme M, Briffa KR. 1993. A comparison of Lamb circulation types with an objective classification scheme. *International Journal of Climatology* **13**: 655–663.

Jones PD, Osborn TJ, Briffa KR. 1997. Estimating sampling errors in large-scale temperature averages. *Journal of Climate* **10**: 2548–2568.

Kalkstein LS, Davis RE. 1989. Weather and human mortality: an evaluation of demographic and inter-regional responses in the U.S. *Annals of the Association of American Geographers* **79**: 44–64.

Kalnay E, Kanamitsu M, Kistler R, Collins W, Deaven D, Gandin L, Iredell M, Saha S, White G, Woollen J, Zhu Y, Chelliah M, Ebisuzaki W, Higgins W, Janowiak J, Mo KC, Ropelewski C, Wang J, Leetmaa A, Reynolds R, Jenne R, Joseph D. 1996. The NCEP/NCAR 40-year reanalysis project. *Bulletin of the American Meteorological Society* **77**: 437–470.

Karl TR, Knight RW. 1997. The 1995 Chicago heat wave: How likely is a recurrence? *Bulletin of the American Meteorological Society* **78**: 1107–1119.

Kettle H, Thompson R. 2004. Statistical downscaling in European mountains: verification of reconstructed air temperature. *Climate Research* **26**: 97–112.

DOI: 10.1002/joc

Kidson JW, Thompson RD. 1998. A comparison of statistical and model-based downscaling techniques for estimating local climate variations. *Journal of Climate* **11**: 735–753.

Kim JW, Chang JT, Baker NL, Wilks DS, Gates WL. 1984. The statistical problem of climate inversion: Determination of the relationship between local and large-scale climate. *Monthly Weather Review* **112**: 2069–2077.

Matalas NC. 1967. Mathematical assessment of synthetic hydrology. *Water Resources Research* **3**: 937–945.

McAveney BJ, Covey C, Joussaume S, Kattsov V, Kitoh A, Ogana W, Pitman AJ, Weaver AJ, Wood RA, Zhao Z-C. 2001. Model evaluation. *Climate Change 2001: The Scientific Basis. Contribution of Working Group I to the Third Assessment Report of the Intergovernmental Panel on Climate Change*, Houghton JT, Ding Y, Griggs DJ, Noguer M, van der Linden PJ, Dai X, Maskell K, Johnson CA (eds). Cambridge University Press: Cambridge, New York, USA; 881.

Meehl GA, Tebaldi C. 2004. More intense, more frequent, and longer lasting heat waves in the 21st century. *Nature* **305**: 994–997.

Mpelasoka FS, Mullan AB, Heerdegen RG. 2001. New Zealand climate change information derived by multivariate statistical and artificial neural network approaches. *International Journal of Climatology* **21**: 1415–1433.

Murphy J. 1999. An evaluation of statistical and dynamical techniques for downscaling local climate. *Journal of Climate* **12**: 2256–2284.

National Assessment Synthesis Team. 2000. Climate Change Impacts on the United States. The Potential Consequences of Climate Variability and Change. US Global Change Research Program (available online from http://www.usgcrp.gov/usgcrp/nacc/default.htm).

Palutikof JP, Goodess CM, Watkins SJ, Holt T. 2002. Generating rainfall and temperature series at multiple sites: Examples from the Mediterranean. *Journal of Climate* **15**: 3529–3548.

Peterson TC, Easterling DR, Karl TR, Groisman P, Nicholls N, Plummer N, Torok S, Auer I, Boehm R, Gullett D, Vincent L, Heino R, Tuomenvirta H, Mestre O, Szentimrey T, Salinger J, Forland EJ, Hanssen-Bauer I, Alexandersson H, Jones P, Parker D. 1998. Homogeneity adjustments of in situ atmospheric climate data: a review. *International Journal of Climatology* **18**: 1493–1517.

Pope VD, Gallani ML, Rowntree PR, Stratton RA. 2000. The impact of new physical parameterizations in the Hadley Centre climate model: HadAM3. *Climate Dynamics* **16**: 123–146.

Portman DA, Wang W-C, Karl TR. 1992. Comparison of general circulation model and observed regional climates: daily and seasonal variability. *Journal of Climate* **5**: 343–353.

Qian B, Hayhoe H, Gameda S. 2005. Evaluation of the stochastic weather generators LARS-WG and AAFC-WG for climate change impact studies, *Climate Research* **29**: 3–21.

Richardson CW, Wright DA. 1984. *WGEN: A Model for Generating Daily Weather Variables*. US Department of Agriculture, Agricultural Research Service, ARS-8, 83p.

Robeson SM. 2002. Relationships between mean and standard deviation of air temperature: Implications for global warming. *Climate Research* **22**: 205–213.

Robinson PJ. 2001. On the definition of a heat wave. *Journal of Applied Meteorology* **40**: 762–775.

Sailor DJ, Li X. 1999. A semiempirical downscaling approach for predicting regional temperature impacts associated with climate change. *Journal of Climate* **12**: 103–114.

Schar C, Vidale PL, Luthi D, Frei C, Haberli C, Liniger MA, Appenzeller C. 2004. The role of increasing temperature variability in European summer heatwaves. *Nature* **427**: 332–336.

Schnur R, Lettenmaier DP. 1998. A case study of statistical downscaling in Australia using weather classification by recursive partitioning. *Journal of Hydrology* **212–213**: 362–379.

Schoof JT, Pryor SC. 2001. Downscaling temperature and precipitation: A comparison of regression-based methods and artificial neural networks. *International Journal of Climatology* **21**: 773–790.

Schoof JT, Robeson SM. 2003. Seasonal and spatial variations of cross-correlation matrices used by stochastic weather generators. *Climate Research* **24**: 95–102.

Schubert S. 1998. Downscaling local extreme temperature changes in south-eastern Australia from the CSIRO MARK2 GCM. *International Journal of Climatology* **18**: 1419–1438.

Smoyer KE. 1998. A comparative analysis of heat waves and associated mortality in St Louis, Missouri – 1980 and 1995. *International Journal of Biometeorology* **42**: 44–50.

Smoyer KE, Rainham DGC, Hewko JN. 2000. Heat-stress-related mortality in five cities in Southern Ontario: 1980–1996. *International Journal of Biometeorology* **44**: 190–197.

Souch C, Grimmond CSB. 2004. Applied Climatology: 'heat waves'. *Progress in Physical Geography* **28**: 599–606.

Sousounis PJ, Albercook GM. 2000. The great lakes region: past, present, and future. In *Preparing for a Changing Climate. The Potential Consequences of Climate Variability and Change*, Sousounis PJ, Bisanz JM.

Uppala SM, Kållberg PW, Simmons AJ, Andrae U, da Costa Bechtold V, Fiorino M, Gibson JK, Haseler J, Hernandez A, Kelly GA, Li X, Onogi K, Saarinen S, Sokka N, Allan RP, Andersson E, Arpe K, Balmaseda MA, Beljaars ACM, van de Berg L, Bidlot J, Bormann N, Caires S, Chevallier F, Dethof A, Dragosavac M, Fisher M, Fuentes M, Hagemann S, Hólm E, Hoskins BJ, Isaksen L, Janssen PAEM, Jenne R, McNally AP, Mahfouf J-F, Morcrette J-J, Rayner NA, Saunders RW, Simon P, Sterl A, Trenberth KE, Untch A, Vasiljevic D, Viterbo P, Woollen J. 2005. The ERA-40 re-analysis. *Quarterly Journal of the Royal Meteorological Society* **131**: 2961–3012.

von Storch H. 1999. On the use of "inflation" in statistical downscaling. *Journal of Climate* **12**: 3505–3506.

Vose RS, Easterling DR, Gleason B. 2005. Maximum and minimum temperature trends for the globe: an update through 2004. *Geophysical Research Letters* **32**: L23822.

Watts JD, Kalkstein LS. 2004. The development of a warm weather relative stress index for environmental applications. *Journal of Applied Meteorology* **43**: 503–513.

Weichert A, Burger G. 1998. Linear versus nonlinear techniques in downscaling. *Climate Research* **10**: 83–93.

Wilby RL, Wigley TML. 1997. Downscaling general circulation model output: a review of methods and limitations. *Progress in Physical Geography* **21**: 530–548.

Wilks DS. 1992. Adapting stochastic weather generation algorithms for climate change studies. *Climatic Change* **22**: 67–84.

Wilks DS. 1999. Interannual variability and extreme-value characteristics of several stochastic daily precipitation models. *Agricultural and Forest Meteorology* **93**: 153–169.

Wilks DS, Wilby RL. 1999. The weather generation game: a review of stochastic weather models. *Progress in Physical Geography* **23**: 329–357.

DOI: 10.1002/joc